SP Science Press

ARTICLE

Comparative Study on Constitutive Models for Flow Behavior of High Strength Aluminum Alloy AA7075 in Hot Stamping

Wang Ning[1],   Andrey Ilinich[2],   Chen Minghe[1],   George Lucky[2],   Guillaume D'Amours[3]

[1]Nanjing University of Aeronautics and Astronautics, Nanjing 210016, China; [2] Ford Motor Company, Dearborn MI-48124, USA; [3]National Research Council of Canada, Chicoutimi G7H 8C3, Canada

Abstract: In hot stamping, the high strength aluminum alloy AA7075 blank was first fully solutionized and then transferred into room temperature tools for stamping and quenching. To characterize the AA7075 alloy hot deformation behavior, tensile tests employing the heating path representative of the hot stamping process were performed over a temperature range of 200~480 ℃ and a strain rate range of 0.01~10 s^{-1}. Modified constitutive models based on the Arrhenius type model, Johnson-Cook model and Zerilli-Armstrong model were proposed and calibrated using the hot tensile test data. The proposed models coupled the effects of strain, strain rate and temperature on flow stress by expressing the model parameters as polynomial functions of strain, strain rate and temperature. The prediction accuracy of the constitutive models for flow stress was evaluated by the mean square error (MSE) and the correlation coefficient R value. The results indicate that the modified Johnson-Cook model can provide the most accurate prediction for the AA7075 hot flow behavior.

Key words: high strength aluminum alloy AA7075; hot tensile flow behavior; constitutive model

AA7075 is a typical Al-Zn-Mg-Cu alloy widely used in aircraft due to its excellent strength-to-weight ratio[1] which also shows great potential in vehicle weight reduction. However, its application is restricted by the low ambient temperature ductility. Hot stamping of AA7075 aluminum sheet alloy was developed for manufacturing complex shape structural components taking the advantage of improved formability at elevated temperatures[2]. In the hot stamping process, the blank was preheated to approximately 480 ℃, fully solutionized, and then rapidly transferred into room temperature tools and stamped. Simultaneous quench was obtained during forming, which is essential to attain the high strength for subsequent artificial aging treatment[3]. Finite element analysis (FEA) has been widely used to simulate metal forming processes. Simulation accuracy largely relies on the constitutive relation, Young's modulus, Lankford parameters and other material properties defined in the FEA model. For the hot stamping FEA case, it is more complicated as a thermo-mechanical coupling process[4]. A constitutive model is required to provide accurate predictions of the flow curves over the wide range of temperature and strain rate in hot stamping[4].

Isothermal hot stretching, compression and torsion tests have been performed over various temperature and strain rate ranges to investigate the AA7075 aluminum alloy's hot deformation behavior[5-14], workability[7,15-22] and microstructure evolution [13,17,19,22-25]. Based on the experimental results, constitutive models such as the power law type equations[12], Arrhenius type equations combined with Zener-Holloman parameter[5,6,17,22,26-30], Johnson-Cook (JC) model[21,25,29,31], Zerilli-Armstrong (ZA) model[31] and artificial neural network (ANN) model[32] were employed to describe the flow behavior of AA7075 at elevated temperatures. The ANN model application is restricted as it is too complicated for FEA integration at present. The

calibrated constants of the same type model varied with material form, heat treatments, temperatures and strain rates applied in different characterization studies.

The Arrhenius type model and JC model are two typical empirical constitutive models commonly used for describing static or dynamic flow behaviors at elevated temperatures. The widely applied Arrhenius type model with Zener-Hollomon parameter is as follows:

$$Z = \dot{\varepsilon} \exp\left(\frac{Q}{RT}\right) \tag{1}$$

$$\dot{\varepsilon} = AF(\sigma) \exp\left(\frac{-Q}{RT}\right) \tag{2}$$

$$F(\sigma) = \begin{cases} \sigma^{n_1}, & \alpha\sigma < 0.8 \\ \exp(\beta\sigma), & \alpha\sigma > 1.2 \\ \left[\sinh(\alpha\sigma)\right]^n, & \text{for all } \sigma \end{cases} \tag{3}$$

$$\sigma = \frac{1}{\alpha} \ln\left\{ (Z/A)^{1/n} + \left[(Z/A)^{2/n} + 1 \right]^{1/2} \right\} \tag{4}$$

where Z is the Zener-Hollomon parameter, $\dot{\varepsilon}$ is the strain rate in s^{-1}, Q is the activation energy of hot deformation in kJ/mol, R is the universal gas constant which is 8.31 J/(mol·K), T is the temperature in K, σ is the equivalent true stress at given strain in MPa, α, β, n, n_1 and A are material constants, and $\alpha = \beta/n_1$. However, the original model is restricted to the prediction for peak flow stress as the strain effect is ignored.

The original JC and its modified models have been widely used in describing constitutive relations for various materials over a wide range of temperature and strain rate, such as steel[33-42], titanium[43,44] and titanium matrix composites[45], aluminum[21,25,29,31,46,47], magnesium[48,49] and other alloys[50]. The original JC model[51] consists of three items expressing the strain hardening, strain rate and temperature dependence:

$$\sigma = \left(A + B\varepsilon^n\right)\left[1 + C\ln\left(\frac{\dot{\varepsilon}}{\dot{\varepsilon}_{\text{ref}}}\right)\right]\left[1 - \left(\frac{T - T_{\text{ref}}}{T_{\text{Melt}} - T_{\text{ref}}}\right)^m\right] \tag{5}$$

where σ, $\dot{\varepsilon}$, and T are the same as those in the Arrhenius type model, T_{ref} is the reference temperature in K, ε is equivalent true plastic strain, T_{Melt} is the material melt temperature in K, $\dot{\varepsilon}_{\text{ref}}$ is the reference strain rate in s^{-1}, A is the yield stress at reference temperature and reference strain rate in MPa, B is the strain hardening coefficient in MPa, n is the strain hardening exponent, C is the strain rate hardening coefficient and m is the temperature softening coefficient. The decoupled effect simplifies the constants acquisition process but usually leads to a loss of prediction accuracy as it assumes constant strain hardening and strain rate hardening at different temperatures.

The ZA model is a physical based model which has been widely applied in flow stress calculation for hot deformation[29,31,37,44]. The original ZA model[52,53] is represented as Eq.(6), which is constructed for face centered cubic (fcc) and body centered cubic (bcc) metals separately:

$$\sigma = \begin{cases} C_0 + C_1\varepsilon^n \exp\left[-C_3 + C_4 T \ln\left(\frac{\dot{\varepsilon}}{\dot{\varepsilon}_{\text{ref}}}\right)\right] + C_5\varepsilon^n & \text{bcc} \\ C_0 + C_2\varepsilon^n \exp\left[-C_3 + C_4 T \ln\left(\frac{\dot{\varepsilon}}{\dot{\varepsilon}_{\text{ref}}}\right)\right] & \text{fcc} \end{cases} \tag{6}$$

where σ, ε, $\dot{\varepsilon}$, $\dot{\varepsilon}_{\text{ref}}$ and T are the same as those in the JC model, C_0, C_1, C_2, C_3, C_4, C_5 and n are material constants. The temperature and strain rate effects are coupled in the ZA model which is usually used to predict stress in the temperature range from room temperature to $0.6T_{\text{Melt}}$ [53].

In the study of Trimble and O'Donnell [29], the constitutive modeling works for AA7075 were summarized. Different models were compared for predicting the flow stress over a temperature range of 250~450 ℃ and a strain rate range of 10^{-3}~10^2 s^{-1}. And a new model was proposed which can provide consistent predictions with the experiment results. It is difficult to establish a unified constitutive model to accurately predict the flow behavior of AA7075 in different forms under various deformation conditions. And few constitutive studies have been performed for AA7075 hot stamping, which need to consider the solution heat treatment and the quench effects. A heating path representative of the hot stamping process is very necessary for the tensile tests to obtain the true stress-true strain curves.

This study aimed to establish a constitutive model for the AA7075 aluminum sheet alloy which covered the deformation conditions (200~480 ℃, 0.01~10 s^{-1}) determined by previous B-pillar hot stamping researches[2,4]. The Arrhenius type model combined with Zener-Holloman parameter, JC model and the physical based ZA model were modified and calibrated to predict the AA7075 flow behavior over the wide range of temperature and strain rate in hot stamping. And the prediction accuracy was evaluated by calculating the mean square error (MSE) and the correlation coefficient R value with the predicted and experimental results.

1 Experiment

1.1 Material properties

The room temperature material properties of the as-received 2 mm thick AA7075-T6 blank for tensile tests are presented in Table 1[2].

1.2 Experimental procedures

The experiment matrix is given in Table 2.

Table 1   As-received material properties of AA7075-T6 [2]

Property	Value
Ultimate tensile strength/MPa	577
Tensile yield strength (0.2% offset)/MPa	531
Uniform elongation/%	8.6
Total elongation/%	11.5
Thermal conductivity/%IACS	32.3
Rockwell B hardness	91

Table 2   Experiment matrix for AA7075 hot tensile test

Condition	Value
Orientation	Longitudinal, diagonal, transverse
Stain rate/s^{-1}	0.01, 0.1, 1, 10
Temperature/ ℃	200, 280, 360, 400, 440, 480

Fig.1a is the tensile specimen geometry designed according to the standard ASTM E08. And Fig.1b shows the grips used in the tensile test.

The heating path and apparatus applied in the tensile tests are shown in Fig.2. A Pyradia furnace was used for supersaturated solid solution treatment (12 min at 500 ℃). In the salt bath, a rapid quench representing the die quench in hot stamping was attained, as shown in Fig.2, which has a comparable cooling rate to die quenching[3]. The salt bath was 20±5 ℃ above the test temperature to compensate for the heat loss during transfer. In the 480 ℃ tensile tests, the samples were transferred directly from
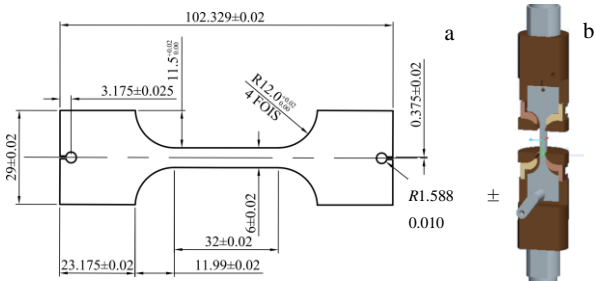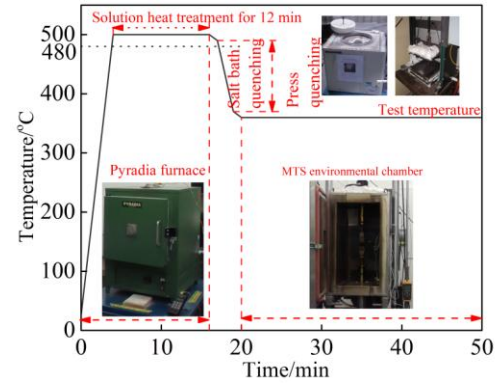

Fig.2   Schematic diagram of the AA7075 hot tensile test heating path

the Pyradia furnace into the environmental chamber and mounted into the grips installed on an MTS RT100 mechanical tensile testing machine.

1.3   Experimental results

The flow curves of different orientations show little difference. So only one representative true stress-true strain curve for each combination of temperature and strain rate is plotted in Fig.3. The strain rate dependence is obvious at 360 ℃ and higher temperatures. And the flow stress drops with increasing the temperature at all strain rates.
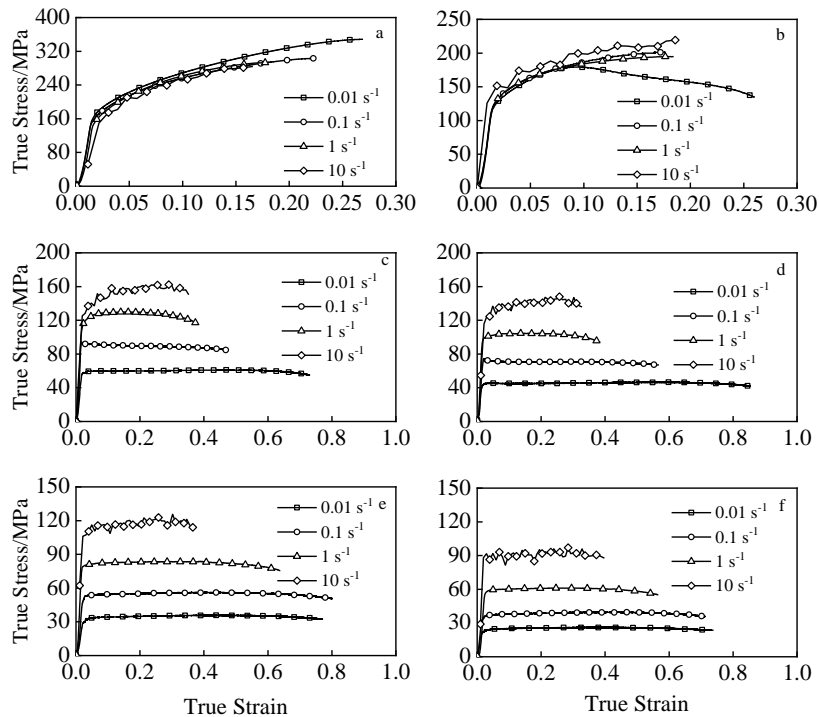

Fig.1   Design of hot tensile test sample (a) and grips (b)

Fig.3   True stress-true strain curves of AA7075-W at different temperatures: (a) 200 ℃, (b) 280 ℃, (c) 360 ℃, (d) 400 ℃, (e) 440 ℃, and (f) 480 ℃

2 Constitutive Models

The true stress and true strain data have been processed by the following steps to obtain true stress versus effective plastic true strain for constitutive modeling:

1) The as-received true stress vs. true strain data was grouped by condition. Data from all samples with the same condition was joined and analyzed together.

2) Strain for one data point was selected to split the data into an elastic portion with strains less than or equal to the selected strain and elastic-plastic portion with strains more than the selected strain.

3) Linear least square (LLS) fit was performed on the elastic data.

4) Quadratic polynomial least square fit was performed using the elastic-plastic data.

5) Steps 2~4 were repeated to find strain point that minimized average residual for both the linear and quadratic fits. Resultant segregation for one condition is shown in Fig.4

6) The effective plastic strain for the elastic-plastic portion was calculated as follows:

$$\varepsilon_{eff} = \varepsilon_{true} - \sigma_{true} / E \qquad (7)$$

7) For constitutive equation fitting, data points were selected on each true stress vs. effective plastic strain curve with a strain interval of 0.02.

The processed true stress vs. effective plastic strain curves and the data points for constitutive equation calibration are shown in Fig.5.

Modified constitutive models based on the Arrhenius type equation combined with Zener-Holloman parameter, JC model and ZA model were proposed and fitted with the true stress vs. effective plastic strain data points given in Fig.5. The reference temperature and strain rate were 473 K and 0.01 s^{-1} for all models, respectively.

2.1 Modified Arrhenius type model

The Arrhenius type equation with Zener-Holloman parameter given by Eq.(1~4) shows that the flow stress can be expressed as a function of α, Z, A and n.
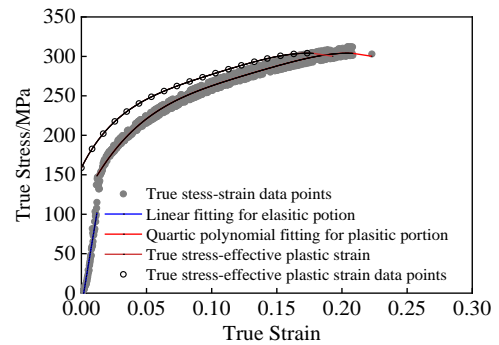

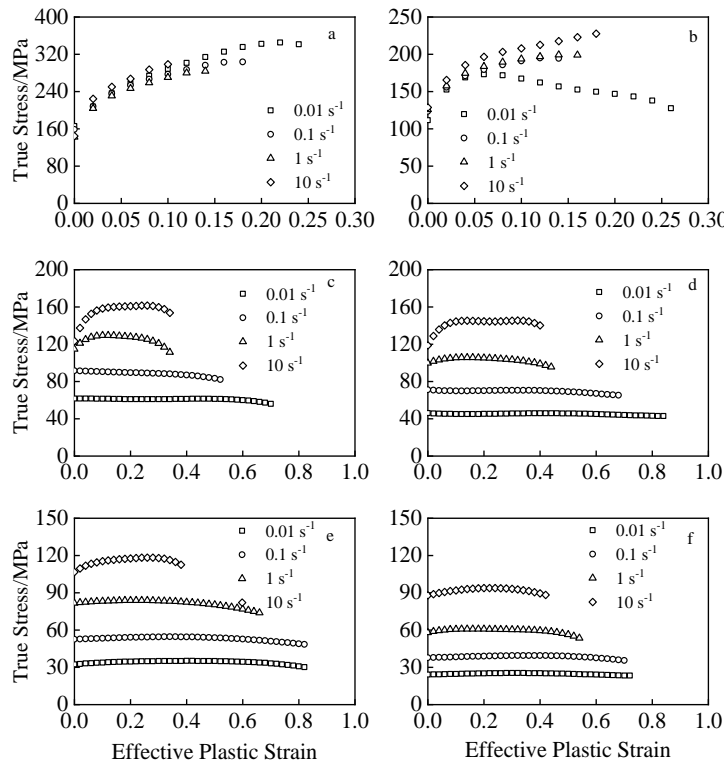Fig.4   Example of calculation of the effective plastic strain at 200 ℃ and 0.1 s^{-1}

Fig.5   True stress versus effective plastic strain curves of AA7075-W at different temperatures: (a) 200 ℃, (b) 280 ℃, (c) 360 ℃, (d) 400 ℃, (e) 440 ℃, and (f) 480 ℃

Replacing $F(\sigma)$ in Eq.(2) with σ^{n_1}, $\exp(\beta\sigma)$ and $[\sinh(\alpha\sigma)]^n$, and taking the natural logarithm on both sides, corresponding relations are obtained:

$$\ln\dot{\varepsilon} = \ln A - \frac{Q}{RT} + n_1 \ln\sigma \tag{8}$$

$$\ln\dot{\varepsilon} = \ln A - \frac{Q}{RT} + \beta\sigma \tag{9}$$

$$\ln\dot{\varepsilon} = \ln A - \frac{Q}{RT} + n\ln\left[\sinh(\alpha\sigma)\right] \tag{10}$$

At a given strain of 0.1, $\ln\sigma$-$\ln\dot{\varepsilon}$ and σ-$\ln\dot{\varepsilon}$ at different temperatures are shown in Fig.6a and Fig.6b, respectively. $1/n_1$ and $1/\beta$ were determined as the slope of the plot by linear fitting. Then α at different temperatures was obtained as $\alpha = \beta/n_1$ which can be expressed as a polynomial function of temperature as follows:

$$\alpha = \sum_{i=1}^{6} \alpha_i T^{6-i} \tag{11}$$

$\ln\left[\sinh(\alpha\sigma)\right]$-$\ln\dot{\varepsilon}$ at different temperatures is plotted as Fig.6c. And $1/n$ is expressed as a polynomial function of temperature:

$$n = 1/\sum_{i=1}^{6} n_i T^{6-i} \tag{12}$$

Taking n into Eq.(10), $Rn\ln\left[\sinh(\alpha\sigma)\right]$-$1/T$ at different strain rates is calculated, as shown in Fig.6d. At a given strain rate, Q is expressed as:

$$Q = \sum_{i=1}^{6} Q_i T^{6-i} \tag{13}$$

The coefficient Q_i is strain rate related:

$$Q_i = \sum_{j=1}^{4} Q_{ij} \ln\dot{\varepsilon}^{4-j} \tag{14}$$

With α, n and Q, $\ln A$ at different temperatures and strain rates can be obtained by Eq.(10) and can be expressed as:

$$A = \exp\left(\sum_{i=1}^{6} A_i T^{6-i}\right) \tag{15}$$

$$A_i = \sum_{j=1}^{4} A_{ij} \ln\dot{\varepsilon}^{4-j} \tag{16}$$

As the strain effect on stress is ignored, the original Arrhenius type equation is usually used to predict the peak stress. Small impact will be made on the stress prediction for steady flow curves at relatively low strain rate and high temperatures, as shown in Fig.5e and 5f. But the strain effect must to be considered because the strain hardening behavior of AA7075 is obvious below 280 ℃, as shown in Fig.5a and 5b. The above calibration process was repeated at the strains ranging from 0 to 0.98 with an interval of 0.02. The data shown in Fig.5 was applied for calibration. And it was assumed that the true stress is constant at the strains between the maximum effective plastic strain and 0.98 for curves which have a maximum strain less than 0.98. The acquired equation coefficients can be expressed as polynomial functions of the effective plastic strain as follows:

$$\alpha_i = \sum_{k=1}^{7} \alpha_{ik} \varepsilon^{7-k} \tag{17}$$

$$n_i = \sum_{k=1}^{7} n_{ik} \varepsilon^{7-k} \tag{18}$$
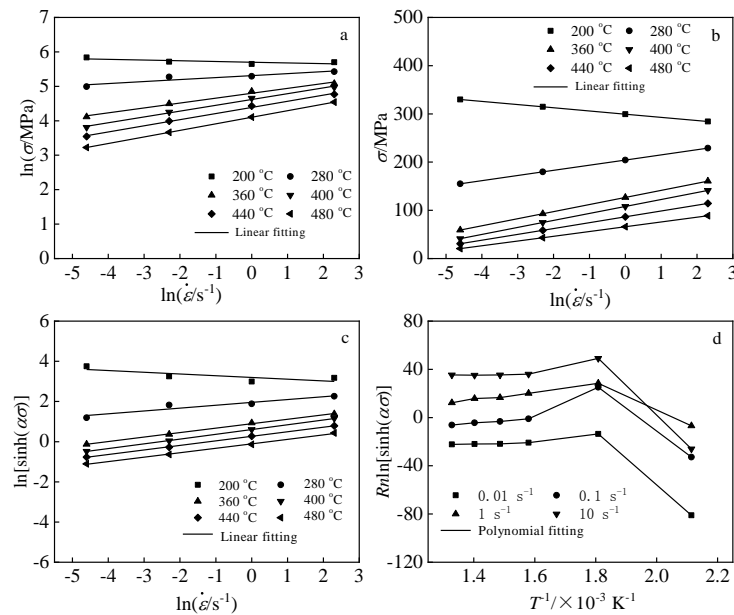
$$Q_{ij} = \sum_{k=1}^{7} Q_{ijk} \varepsilon^{7-k} \tag{19}$$

Fig.6   Plots of $\ln\sigma$-$\ln\dot{\varepsilon}$ (a), σ-$\ln\dot{\varepsilon}$ (b), $\ln\left[\sinh(\alpha\sigma)\right]$-$\ln\dot{\varepsilon}$ (c) and $Rn\ln\left[\sinh(\alpha\sigma)\right]$-$1/T$ (d) at strain of 0.1

$$A_{ij} = \sum_{k=1}^{7} A_{ijk} \varepsilon^{7-k} \tag{20}$$

The constitutive relation is given by Eq.(4) and the parameters are defined as functions of temperature, strain rate and strain, as expressed in Eq.(11~20). The calibrated model constants are plotted in Fig.7, where $P1 \sim P6$, $P7 \sim P12$, $P13 \sim P18$ and $P19 \sim P24$ represent α_{ik}, n_{ik}, Q_{ijk} and A_{ijk}, respectively.

2.2 Modified Johnson-Cook model

The strain hardening is defined by a power law equation in the original JC model as Eq.(5). And the strain, strain rate and temperature effects are isolated. Lin et al[36] proposed a modified JC model employing a quadratic polynomial function for strain hardening and an exponential term, which couples the strain rate and temperature effects as follows:
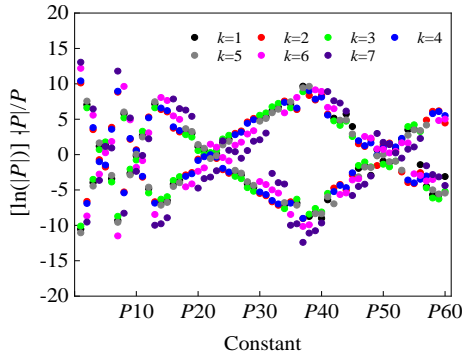

$$\sigma = \left(A_1 + B_1\varepsilon + B_2\varepsilon^2\right)\left(1 + C_1 \ln \dot{\varepsilon}^*\right)\exp\left[\left(\lambda_1 + \lambda_2 \ln \dot{\varepsilon}^*\right)T^*\right] \tag{21}$$

where A_1, B_1, B_2, C_1, λ_1 and λ_2 are constants, $T^* = T - T_{\text{ref}}$, $\dot{\varepsilon}^* = \dot{\varepsilon}/\dot{\varepsilon}_{\text{ref}}$. The flow behavior of a typical high-strength alloy steel at high temperatures was accurately predicted with the modified JC model. Trimble et al[29] also applied it to predict the AA7075 hot compression flow curves but the prediction was not accurate over the entire strain rate and temperature range.

In both the original and modified JC models, it was assumed that the strain hardening is constant at different temperatures and strain rates. And the coefficients were fitted with the flow curve at the reference strain rate and temperature. In the constitutive studies performed by Trimble[29] and Lin et al[36], the flow curves were consistently steady or linearly increased under all conditions, which is suited to employ the fixed strain hardening constants. However, the AA7075 hot stamping deformation behavior in this study is very different as obvious nonlinear strain hardening was observed below 280 ℃ and at strain rate of 10 s^{-1} at 360 and 400 ℃, as shown in Fig.3. The strain hardening constants should be temperature and strain rate dependent.

Based on the quadratic polynomial form strain hardening item proposed by Lin et al[36], the flow curve of each combination of temperature and strain rate can be fitted with the polynomial equation as follows:

$$\sigma = A_1\varepsilon^4 + A_2\varepsilon^3 + A_3\varepsilon^2 + A_4\varepsilon + A_5 \tag{22}$$

A_i vs. $\ln \dot{\varepsilon}^*$ is plotted in Fig.8.

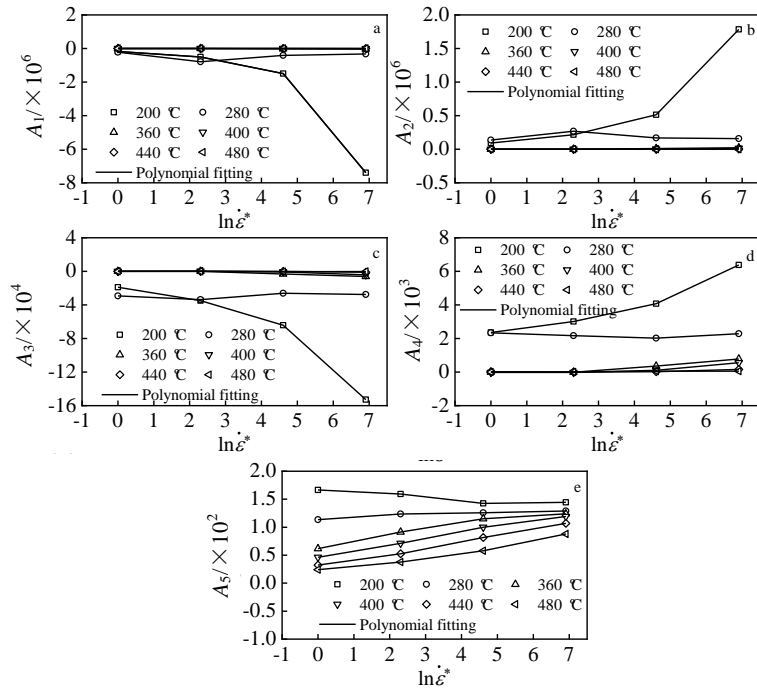Fig.7 Calibrated constants of the modified Arrhenius type model

Fig.8 Plots of A_i-$\ln \dot{\varepsilon}^*$: (a) A_1-$\ln \dot{\varepsilon}^*$, (b) A_2-$\ln \dot{\varepsilon}^*$, (c) A_3-$\ln \dot{\varepsilon}^*$, (d) A_4-$\ln \dot{\varepsilon}^*$, and (e) A_5-$\ln \dot{\varepsilon}^*$

For each temperature, A_i-$\ln\dot{\varepsilon}^*$ was fitted with a polynomial equation:

$$A_i = \sum_{j=1}^{4} A_{ij} \ln \dot{\varepsilon}^{*4-j} \tag{23}$$

The parameter A_{ij} in Eq.(23) is temperature dependent and can be expressed as:

$$A_{ij} = \sum_{k=1}^{6} A_{ijk} T^{*6-k} \tag{24}$$

where $T^* = (T - T_{\text{ref}})/(T_{\text{Melt}} - T_{\text{ref}})$ and $T_{\text{Melt}} = 893$ K.

The strain, strain rate and temperature effects are coupled in the proposed model as Eq.(22~24). The calibrated equation constants are plotted in Fig.9, where $P1 \sim P20$ represent A_{ijk}.

2.3 Modified Zerilli-Armstrong model

Samantaray et al[37] modified the original ZA model and successfully applied it in stress prediction for a titanium-modified austenitic stainless steel and a modified 9Cr–1Mo steel[33]. The modified model is as follows:

$$\sigma = (C_1 + C_2\varepsilon^n)\exp\left[-(C_3 + C_4\varepsilon)T^* + (C_5 + C_6T^*)\ln\dot{\varepsilon}^*\right] \tag{25}$$

where C_1, C_2, C_3, C_4, C_5, C_6 and n are constants. The flow curve at reference temperature and strain rate was employed to calibrate the strain hardening coefficients C_1, C_2 and n which were assumed consistent under all conditions. Zhan[44], Li[54], Trimble[29], and Li et al[55] employed this modified ZA model for predicting the flow behavior of titanium alloy, aluminum alloy and steel. But the prediction accuracy decreases for higher strain rates and lower temperatures at which the flow curves show strong strain hardening behavior.

Based on the modified ZA model given in Eq.(25), a model coupling the strain, strain rate and temperature effect can be proposed:

$$\sigma = A(\varepsilon, \ln\dot{\varepsilon}^*)\exp\left[B(\varepsilon, \ln\dot{\varepsilon}^*, T^*) + C(\varepsilon, T^*)\ln\dot{\varepsilon}^*\right] \tag{26}$$

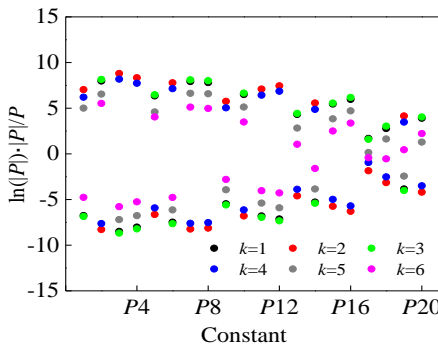Taking the natural logarithm on both sides, it can be expressed as:

$$\ln\sigma = \ln\left[A(\varepsilon, \ln\dot{\varepsilon}^*)\right] + B(\varepsilon, \ln\dot{\varepsilon}^*, T^*) + C(\varepsilon, T^*)\ln\dot{\varepsilon}^* \tag{27}$$

$\ln\sigma$-$\ln\dot{\varepsilon}^*$ at a given strain of 0.1 for different temperatures is plotted in Fig.10. And $C(\varepsilon, T^*)$ is the slope of $\ln\sigma$-$\ln\dot{\varepsilon}^*$.

As shown in Fig.11, $C(\varepsilon, T^*)$ can be expressed as a polynomial function of ε and T^*:

$$C(\varepsilon, T^*) = \sum_{i=0, j=0}^{5,3,i+j\leq5} C_{ij}\varepsilon^i T^{*j} \tag{28}$$

$\left[\ln\sigma - C(\varepsilon, T^*)\ln\dot{\varepsilon}^*\right]$-$T^*$ at a given strain of 0.1 at different strain rates is plotted in Fig.12. $\ln\sigma - C(\varepsilon, T^*)\ln\dot{\varepsilon}^*$ can be expressed as a polynomial function of T^*:

$$\ln\sigma - C(\varepsilon, T^*)\ln\dot{\varepsilon}^* T^* = \sum_{i=1}^{4} D_i(\varepsilon, \ln\dot{\varepsilon}^*)T^{*4-i} \tag{29}$$
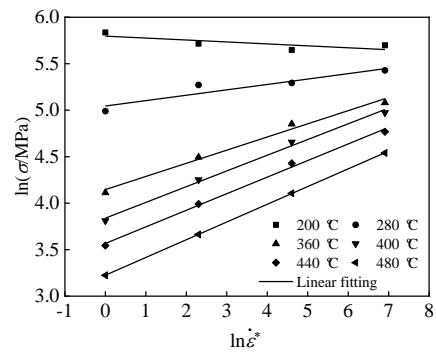

Fig.10   Plots of $\ln\sigma$-$\ln\dot{\varepsilon}^*$ at strain of 0.1
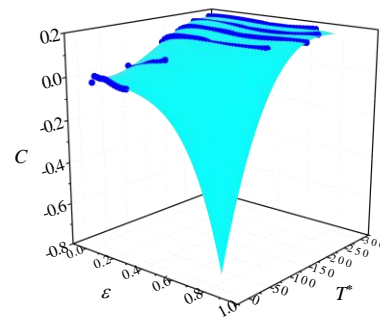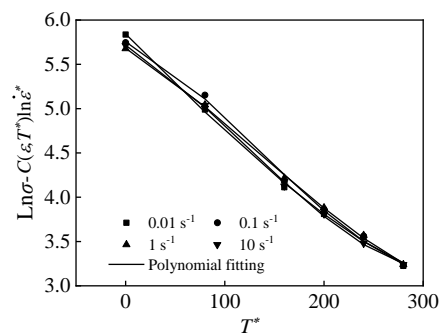

Fig.11   Plots of C-ε, T^*

Fig.9   Calibrated constants of modified JC model

Fig.12   Plots of $\left[\ln\sigma - C(\varepsilon, T^*)\ln\dot{\varepsilon}^*\right]$-$T^*$ at strain of 0.1
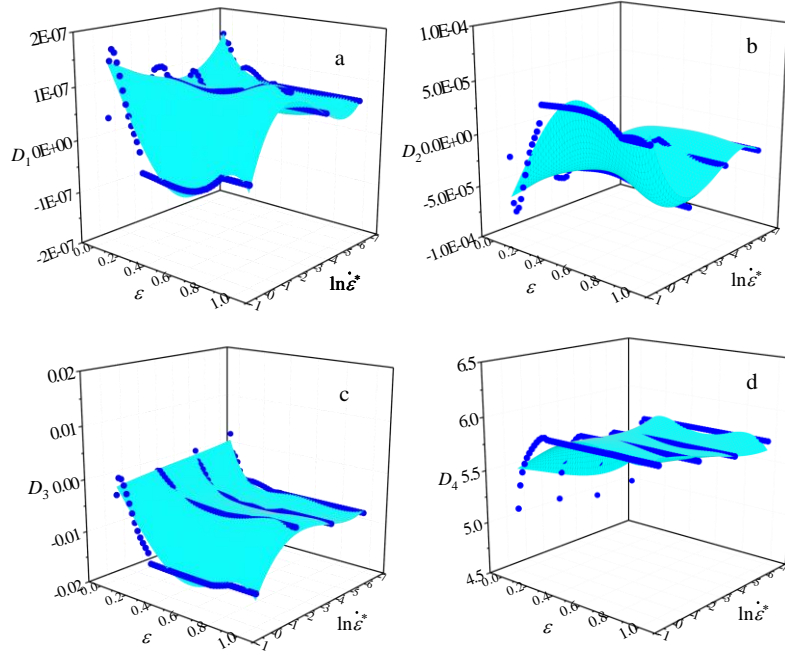
Fig.13 Plots of D_n-ε, $\ln \dot{\varepsilon}^*$: (a) D_1-ε, $\ln \dot{\varepsilon}^*$, (b) D_2-ε, $\ln \dot{\varepsilon}^*$, (c) D_3-ε, $\ln \dot{\varepsilon}^*$ and (d) D_4-ε, $\ln \dot{\varepsilon}^*$

$B\left(\varepsilon, \ln \dot{\varepsilon}^*, T^*\right)$ and $A\left(\varepsilon, \ln \dot{\varepsilon}^*\right)$ can be expressed as:

$$B\left(\varepsilon, \ln \dot{\varepsilon}^*, T^*\right)^* = \sum_{i=1}^{3} D_i \left(\varepsilon, \ln \varepsilon^*\right) T^{*4-i} \qquad (30)$$

$$A\left(\varepsilon, \ln \dot{\varepsilon}^*\right) = \exp\left[D_4 \left(\varepsilon, \ln \dot{\varepsilon}^*\right)\right] \qquad (31)$$

As shown in Fig.13, $D_n\left(\varepsilon, \ln \dot{\varepsilon}^*\right)$-$\varepsilon$ and $\ln \dot{\varepsilon}^*$ is fitted with a polynomial equation:

$$D_n \left(\varepsilon, \ln \varepsilon^*\right) = \sum_{i=0, j=0}^{5,3, i+j \leq 5} D_{nij} \varepsilon^i \ln \varepsilon^{*j} \qquad (32)$$

The calibrated constants of the modified ZA model are plotted in Fig.14, where $P1 \sim P18$ represent $ij\left(i = 0 \sim 5, j = 0 \sim 3, i+j \leq 5\right)$.
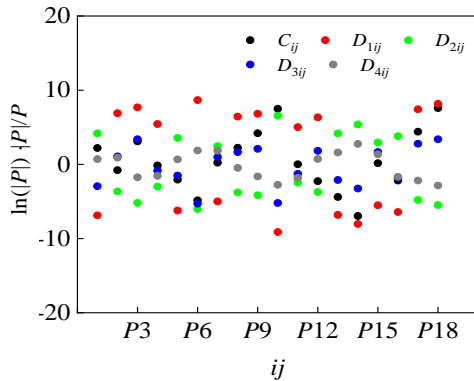
3   Results and Discussion

Fig.14   Calibrated constants of the modified ZA model

The flow curves predicted by the proposed models are compared with the experimental results, as shown in Fig.15.

To evaluate the model prediction accuracy, the MSE and correlation coefficient R value of each model are calculated using Eq.(33) and Eq.(34):

$$\text{MSE} = \frac{1}{n} \sum_{i=1}^{n} \left(\hat{\sigma}_i - \sigma_i\right)^2 \qquad (33)$$

$$R = \frac{\sum_{i=1}^{n} \left(\sigma_i - \bar{\sigma}\right)\left(\hat{\sigma}_i - \bar{\hat{\sigma}}\right)}{\sqrt{\sum_{i=1}^{n} \left(\sigma_i - \bar{\sigma}\right)^2 \sum_{i=1}^{n} \left(\hat{\sigma}_i - \bar{\hat{\sigma}}\right)^2}} \qquad (34)$$

where n is the number of picked data points of one true stress vs. effective plastic strain curve, σ and $\hat{\sigma}$ are the experimental and predicted true stress in MPa, and $\bar{\sigma}$ and $\bar{\hat{\sigma}}$ are the mean experimental and predicted true stresses in MPa, respectively. The results are plotted in Fig.16 and Fig.17.

The modified Arrhenius model MSE for the entire tensile dataset is 43.00 and the R value is 0.9955. The prediction is in good agreement with the experiment for temperatures above 280 ℃. Fig.16a shows that the prediction accuracy decreases for the stress above 150 MPa. The MSE for each temperature and strain rate shown in Fig.17a indicates that the prediction accuracy increases for higher temperature. The strain hardening is not well described though the strain effect is coupled by introducing strain related polynomial functions. A more precise relation needs to be defined to couple the strain effect.

The total MSE of the modified JC model is 0.0715 and R value is almost 1. The correlation between the experiments and predictions shown in Fig.16b shows that the predicted

results are in good accordance with the experimental results. The effects of strain, strain rate and temperature are well described by the polynomial functions.

The total MSE of the modified ZA model is 27.40 and the

R value is 0.9967. The model can provide good predictions for most flow curves. But the accuracy is lower than that of the modified JC model. The MSE for each strain rate and temperature is shown in Fig.17c.
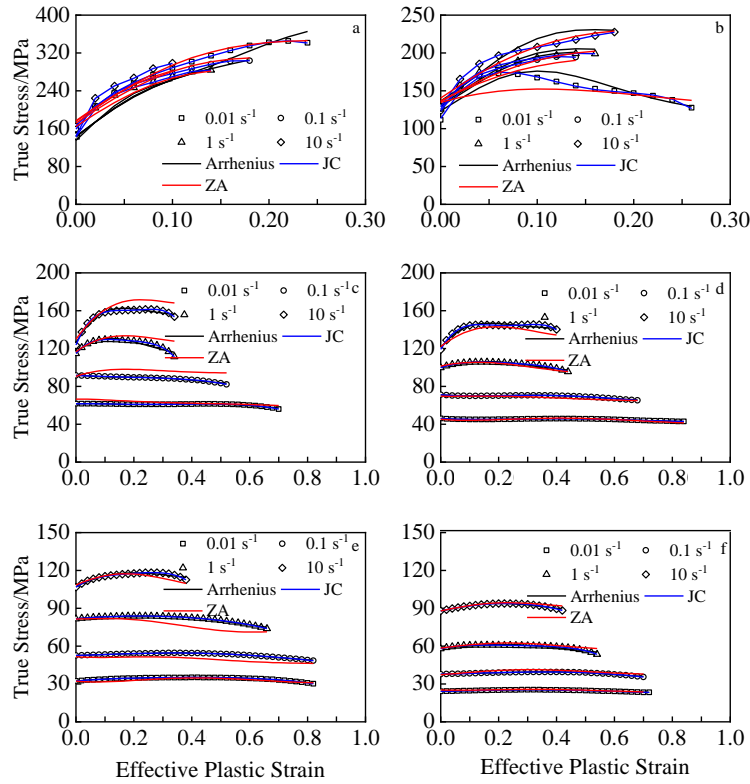

Fig.15   Predicted true stress versus true strain curves using the modified models: (a) 200 ℃, (b) 280 ℃, (c) 360 ℃, (d) 400 ℃, (e) 440 ℃, and (f) 480 ℃
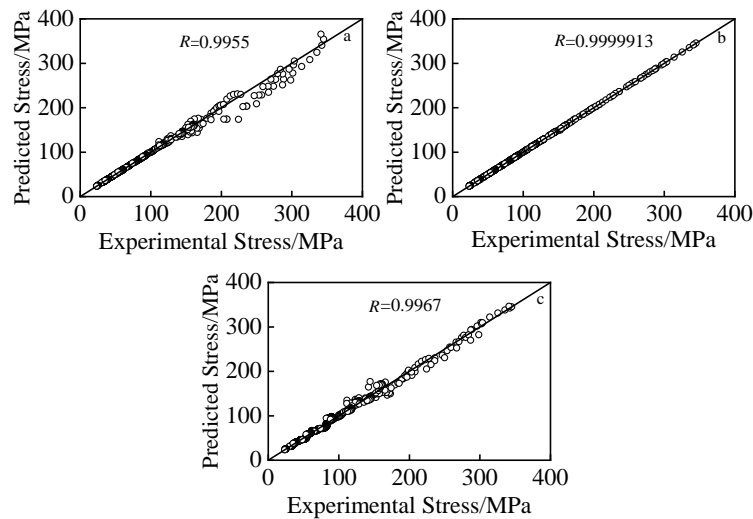

Fig.16   Correlation between the predicted stress by the modified Arrhenius type (a), JC (b) and ZA (c) models and the experimental results
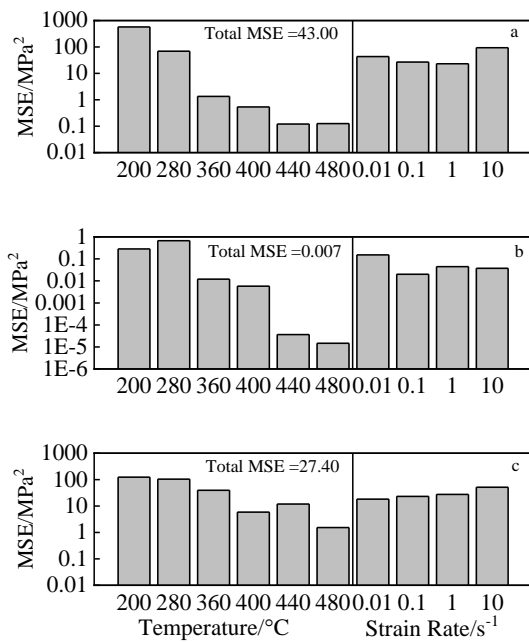
Fig.17   MSE of the modified Arrhenius type (a), JC (b) and ZA (c) models at different temperatures and strain rates

4   Conclusions

1) The modified Arrhenius type equation combined with Zener-Holloman parameter can provide accurate predictions for the stress at lower strain rates and higher temperatures. The prediction accuracy is improved with increasing the temperature. The strain effects can be coupled by applying polynomial equations for expressing the model parameters.

2) The modified JC model provides the best prediction by replacing the original strain hardening item with a polynomial function. The strain, strain rate and temperature effects can be coupled by expressing the strain hardening coefficients as a polynomial equation of temperature and strain rate. The modified JC model can provide an adequately accurate description for the hot tensile behavior of the AA7075 sheet alloy.

3) The modified ZA model can provide better prediction than the modified Arrhenius type equation in describing flow behavior at 200 ℃. Fewer constants need to be calibrated and the prediction results are not consistently precise.

References

1   Jr E A S, Staley J T. *Progress in Aerospace Sciences*[J], 1996, 32(2): 131

2   Harrison N R, Luckey S G. *SAE International Journal of Materials and Manufacturing*[J], 2014, 7(3): 567

3   Keci A, Harrison N R, Luckey S G. *SAE Technical Papers*[J], 2014(1): 984

4   Ilinich A, Luckey S G. *SAE Technical Papers*[J], 2014(1): 983

5   Hashimoto S. *Thesis for Master*[D]. Massachusetts: Massachusetts Institute of Technology, 1986

6   Rus A L. *Metalurgia*[J], 2014, 66(4): 15

7   Jenab A, Taheri A K. *International Journal of Mechanical Sciences*[J], 2014, 78(1): 97

8   Beland J F, D'Amours G. *SAE Technical Papers*[J], 2012(1): 539

9   Zhou M, Lin Y C, Deng J *et al. Materials and Design*[J], 2014, 59: 141

10   Lee W S, Sue W C, Lin C F *et al. Journal of Materials Processing Technology*[J], 2000, 100(1): 116

11   Zhang H, Lin G Y, Peng D S *et al. Journal of Materials Processing Technology*[J], 2004, 148(2): 245

12   Quan G Z, Liu K W, Zhou J *et al. Transactions of Nonferrous Metals Society of China*[J], 2009, 19(S3): 537

13   Sun Z C, Zheng L S, Yang H. *Materials Characterization*[J], 2014, 90(4): 71

14   Sakai T, Takahashi C. *Materials Transactions JIM*[J], 1991, 32(5): 369

15   Rajamuthamilselvan M, Ramanathan S. *Journal of Alloys and Compounds*[J], 2011, 509(3): 948

16   Taheri-Mandarjani M, Zarei-Hanzaki A, Abedi H R. *Materials Science and Engineering A*[J], 2015, 637: 107

17   Wang L, Yu H, Lee Y *et al. Metals and Materials International*[J], 2015, 21(5): 832

18   Hui W, Luo Y B, Friedman P *et al. Transactions of Nonferrous Metals Society of China*[J], 2012, 22(1): 1

19   Lin Y C, Li L T, Xia Y C *et al. Journal of Alloys and Compounds*[J], 2013, 550(6): 438

20   Puchi-Cabrera E S, St, Ochoa-Perez E *et al. Materials Science and Engineering A*[J], 2011, 528(3): 895

21   Senthila K,Iqbala M A, Chandel P S *et al. International Journal of Impact Engineering*[J], 2017, 108: 171

22   Cerri E, Evangelista E, Forcellese A *et al. Materials Science and Engineering A*[J], 1995, 197(2): 181

23   Rokni M R, Zarei-Hanzaki A, Roostaei A A *et al. Materials and Design*[J], 2011, 32(4): 2339

24   Wang L, Yu H, Lee Y S *et al. Materials Science and Engineering A*[J], 2016, 652: 221

25   Lin Y C, Li L T, Fu Y X *et al. Journal of Materials Science*[J], 2012, 47(3): 1306

26   Sheppard T, Jackson A. *Materials Science and Technology*[J], 1997, 13(3): 203

27   Rokni M R, Zarei-Hanzaki A, Roostaei A A *et al. Materials and Design*[J], 2011, 32(10): 4955

28   Mirzadeh H. *Journal of Materials Engineering and Performance*[J], 2015, 24(3): 1095

29   Trimble D, O'Donnell G E. *Materials and Design*[J], 2015, 76: 150

30   Quan G Z, Mao Y P, Li G S *et al. Computational Materials Science*[J], 2012, 55: 65

31   Paturi U M R, Narala S K R, Pundir R S. *Materials Science*

   and Engineering A[J], 2014, 605(6): 176

32 Sheikh-Ahmad J, Twomey J. *Journal of Materials Processing Technology*[J], 2007, 186(1): 339

33 Samantaray D, Mandal S, Bhaduri A K. *Computational Materials Science*[J], 2009, 47(2): 568

34 Wang Y P, Han C, Wang C *et al*. *Journal of Materials Science*[J], 2011, 46(9): 2922

35 Zhang Q, Qiang C, Zhang X. *Journal of Materials Engineering and Performance*[J], 2014, 23(12): 4336

36 Lin Y C, Chen X M, Liu G. *Materials Science and Engineering A*[J], 2010, 527(26): 6980

37 Samantaray D, Mandal S, Borah U *et al*. *Materials Science and Engineering A*[J], 2009, 526(1-2): 1

38 Gambirasio L, Rizzi E. *Computational Materials Science*[J], 2016, 113: 231

39 Prawoto Y, Fanone M, Shahedi S *et al*. *Computational Materials Science*[J], 2012, 54(1): 48

40 Li H, He L, Zhao G *et al*. *Materials Science and Engineering A*[J], 2013, 580: 330

41 Wang X, Chandrashekhara K, Rummel S A *et al*. *Journal of Materials Science*[J], 2017, 52(5): 2800

42 Li H, Wang X, Duan J *et al*. *Materials Science and Engineering A*[J], 2013, 577: 138

43 Cai J, Wang K, Zhai P *et al*. *Journal of Materials Engineering and Performance*[J], 2015, 24(1): 32

44 Zhan Hongyi, Wang G, Kent D *et al*. *Materials Science and Engineering A*[J], 2014, 612: 71

45 Song W, Ning J, Mao X *et al*. *Materials Science and Engineering A*[J], 2013, 576: 280

46 Lin Y C, Ding Y, Chen M S *et al*. *Materials and Design*[J], 2013, 52(24): 118

47 Maheshwari A K, Pathak K K, Ramakrishnan N *et al*. *Journal of Materials Science*[J], 2010, 45(4): 859

48 Abbasi-Bani A, Zarei-Hanzaki A, Pishbin M H *et al*. *Mechanics of Materials*[J], 2014, 71: 52

49 Hou Q Y, Wang J T. *Computational Materials Science*[J], 2010, 50(1): 147

50 Wang X, Huang C, Zou B *et al*. *Materials Science and Engineering A*[J], 2013, 580: 385

51 Johnson G R, Cook W H. *Proceedings of the 7th International Symposium on Ballistics*[C]. Hague: International Ballistics Society, 1983: 541

52 Zerilli F J, Armstrong R W. *Journal of Applied Physics*[J], 1987, 61(5): 1816

53 Lin Y C, Chen X M. *Computational Materials Science*[J], 2010, 49(3): 628

54 Li J, Li F, Cai J *et al*. *Computational Materials Science*[J], 2013, 71(3): 56

55 Li H Y, Li Y H, Wang X F *et al*. *Materials and Design*[J], 2013, 49: 493

AA7075 高强铝合金热冲压流变行为本构模型对比研究

王　宁[1]，Andrey Ilinich[2]，陈明和[1]，George Lucky[2]，Guillaume D'Amours[3]

(1. 南京航空航天大学，江苏　南京　210016)

(2. 福特汽车公司，美国　密歇根　迪尔伯恩　MI-48124)

(3. 加拿大国家研究委员会，加拿大　魁北克　希库蒂米　G7H 8C3)

摘　要：在热冲压过程中，AA7075 高强铝合金板料经充分固溶后移入室温模具进行冲压成形并淬火。为表征 AA7075 铝合金在热冲压工艺中的变形行为，在温度 200~480 ℃、应变速率 0.01~10 s^{-1} 范围内进行了高温拉伸试验。基于 Arrhenius 类型本构模型、Johnson-Cook 模型以及 Zerilli-Armstrong 模型提出了多种修正本构模型，并应用实验所获流变曲线进行了拟合。提出的修正模型通过将模型参数表示为应变、应变速率及温度相关的多项式函数耦合了应变、应变速率及温度对流变应力的影响，并通过均方误差（MSE）以及相关系数 *R* 值对模型流变应力预测准确性进行了评价。结果表明，修正的 Johnson-Cook 模型能够更加准确的预测 AA7075 高温流变行为。

关键词：AA7075高强铝合金；热拉伸流变行为；本构模型

作者简介：王　宁，男，1987 年生，博士，南京航空航天大学机电学院，江苏　南京　210016，E-mail: meewn1987@nuaa.edu.cn